

Federated Learning for THz Channel Estimation

Ahmet M. Elbir, *Senior Member, IEEE*, Wei Shi, *Member, IEEE*, Kumar Vijay Mishra, *Senior Member, IEEE*, and Symeon Chatzinotas, *Senior Member, IEEE*

Abstract

This paper addresses two major challenges in terahertz (THz) channel estimation: the beam-split phenomenon, i.e., beam misalignment because of frequency-independent analog beamformers, and computational complexity because of the usage of ultra-massive number of antennas to compensate propagation losses. Data-driven techniques are known to mitigate the complexity of this problem but usually require the transmission of the datasets from the users to a central server entailing huge communications overhead. In this work, we employ federated learning (FL), wherein the users transmit only the model parameters instead of the whole dataset, for THz channel estimation to improve the communications-efficiency. In order to accurately estimate the channel despite beam-split, we propose a beamspace support alignment technique without requiring additional hardware. Compared to the previous works, our method provides higher channel estimation accuracy as well as approximately 68 times lower communications overhead.

Index Terms

Beam split, channel estimation, federated learning, support recovery, Terahertz.

I. INTRODUCTION

The fifth-generation (5G) wireless networks that employ millimeter-wave (mm-Wave) frequencies are moving closer to operational deployment. The lessons learned from the previous and

This work was supported in part by the Natural Sciences and Engineering Research Council of Canada (NSERC), Ericsson Canada, and the ERC Project AGNOSTIC.

A. M. Elbir is with Interdisciplinary Centre for Security, Reliability and Trust (SnT) at the University of Luxembourg, Luxembourg (e-mail: ahmetmelbir@gmail.com).

W. Shi is with the School of Information Technology, Carleton University, Ottawa, Canada (e-mail: wei.shi@carleton.ca).

K. V. Mishra is with the United States Army Research Laboratory, Adelphi, MD 20783 USA (e-mail: kvm@ieee.org).

S. Chatzinotas is with the SnT at the University of Luxembourg, Luxembourg (e-mail: symeon.chatzinotas@uni.lu).

ongoing 5G research are paving way for conceptualization of 6G technologies for developing technologies for Terahertz (THz) band [1]. Whereas 5G systems incorporate massive multiple-input multiple-output (MIMO) configurations, 6G networks are envisaged to operate at higher frequencies (up to 10 THz) to exploit high-capacity data transmission with wider bandwidth using ultra-massive (UM) MIMO architectures.

The definition of the THz band varies among different IEEE communities [2]. In general, recent works on wireless communications usually define this band as 0.1 – 10 THz with a large overlap with mm-Wave frequencies (e.g., 0.03 – 0.3 THz) [3]. Compared to mm-Wave frequencies, the wireless communications in THz band faces several challenges, e.g., spreading loss, molecular absorption and shorter range, hence it should be dealt with techniques that are developed by taking into account these challenges [4]. The THz channels are extremely sparse and modeled as line-of-sight (LoS)-dominant and non-LoS (NLoS)-assisted models [3–5]. On the other hand, both LoS and NLoS paths are significant in the mm-Wave channel [6]. Furthermore, the use of frequency-independent analog beamformers, *beam-split* phenomenon occurs in THz-bands, i.e., the generated beams split into different physical directions (see, e.g., Fig. 1, [2, Fig.11] and [7, Fig.4] for illustration) at each subcarrier because of ultra-wide bandwidth and large number of antennas [5].

With the aforementioned unique peculiarities, THz channel estimation is a challenging problem. In prior works, the beam-split effect remains relatively unexamined [8–11]. Specifically, beam-split causes enough deviations in the spatial channel directions at different subcarriers, producing separation in the angular domain [12]. At mm-Wave, *beam-squint* is broadly used to describe the same phenomenon [2, 6]). While [13] and [7] employ time-delay networks as an additional hardware component to mitigate the beam-split, signal processing techniques have also been considered [2]. For instance, [12] developed a beam-split pattern detection (BSPD) technique to recover the channel support among subcarriers and construct a one-to-one match for the physical channel direction.

Besides the above model-based techniques, data-driven model-free approaches, e.g., machine learning (ML), have also been suggested for THz channel estimation [14–16]. In particular, ML-based models, e.g., multilayer perceptron (MLP) [16], deep convolutional neural network (DCNN) [15], and deep kernel learning (DKL) [14], have been introduced to lower the computational complexity arising from UM-MIMO architectures. However, all of these works consider a narrowband scenario, which does not exploit the key drivers of wide bandwidths in the THz

band. Furthermore, the ML-based techniques involve the transmission of the datasets to a central parameter server (PS), entailing huge communications overhead. In order to reduce the amount of transmitted data, federated learning (FL)-based channel estimation is proposed in [17], wherein the CNN parameters are computed at the users and, in place of the datasets, these parameters are sent to the PS for model aggregation. Compared to centralized learning (CL) models, FL-based approaches are reported to have approximately 20-30 times lower the communications overhead [17–19]. However, [17] only considers mm-Wave channel estimation and the effect of beam-split is not taken into account.

In this paper, we present an FL-based THz channel estimation approach that is robust to beam-split. In particular, we introduce beamspace support alignment (BSA) technique in which we first convert the received signal to beamspace, wherein the amount of angular deviation because of beam-split is determined based on the mismatch between the central and subcarrier frequencies. Then, the beamspace spectra of subcarriers are shifted and combined to generate a single spectrum such that the channel supports are aligned. Next, we design a CNN model trained on local datasets of the users. The input of the CNN is the received pilot signals in the downlink collected after analog beamformer while the output/label data is the channel matrix. Previous works on ML/FL-based channel estimation assume that the label is selected as the true channel matrix, which is actually not available practically (see, e.g., [14–17] and the references therein). Contrary to these approaches, we consider a more practical method in which the minimum mean-squared-error (MMSE) and BSA techniques are used to obtain the label instead of selecting it as the true channel matrix.

Notation: Throughout the paper, $(\cdot)^\top$ and $(\cdot)^\text{H}$ denote the transpose and conjugate transpose operations, respectively. For a matrix \mathbf{A} , \mathbf{A}_n and \mathbf{A}^\dagger correspond to the n th column and the Moore-Penrose pseudo-inverse of \mathbf{A} , respectively. $\lceil \cdot \rceil$ is the ceiling operator, ∇ represents the gradient operation. $\|\cdot\|_0$, $\|\cdot\|_1$, $\|\cdot\|_2$ and $\|\cdot\|_{\mathcal{F}}$ denote the l_0 , l_1 , l_2 and Frobenius norms, respectively.

II. SIGNAL MODEL AND PROBLEM FORMULATION

Consider a wideband ultra-massive MIMO architecture, wherein the base station (BS) is equipped with N_{T} antennas and N_{RF} radio-frequency (RF) chains to serve K single-antenna users. In the downlink, the BS employs frequency-dependent baseband beamformer $\mathbf{F}_{\text{BB}}[m] \in \mathbb{C}^{K \times K}$ to process the vector of transmitted signals $\mathbf{s}[m] = [s_1[m], \dots, s_K[m]]^\top$ ($m \in \mathcal{M} =$

$\{1, \dots, M\}$). Then, frequency-independent analog beamformers $\mathbf{F}_{\text{RF}} \in \mathbb{C}^{N_{\text{T}} \times N_{\text{RF}}}$ ($N_{\text{RF}} = K < N_{\text{T}}$) realized with phase-shifters are used to steer the generated beams toward users. Therefore, \mathbf{F}_{RF} has unit-modulus constraint, i.e., $|[\mathbf{F}_{\text{RF}}]_{i,j}| = \frac{1}{\sqrt{N_{\text{T}}}}$ as $i = 1, \dots, N_{\text{RF}}$ and $j = 1, \dots, N_{\text{T}}$. Let us define the transmitted signal as

$$\mathbf{z}[m] = \mathbf{F}_{\text{RF}} \mathbf{F}_{\text{BB}}[m] \mathbf{s}[m], \quad (1)$$

, then the received signal at the k th user in the m th subcarrier is

$$y_k[m] = \mathbf{h}_k^{\text{T}}[m] \mathbf{z}[m] + n_k[m], \quad (2)$$

where $n_k[m] \in \mathbb{C}$ denotes the additive white Gaussian noise (AWGN) vector with $\mathbf{n}_k[m] \sim \mathcal{CN}(0, \sigma_n^2)$.

In THz transmission, the wireless channel is modeled as the superposition of a single LoS path and the contribution of a few NLoS paths, which are small due to large reflection loses, scattering and refraction [3–5]. Then, the $N_{\text{T}} \times 1$ THz channel vector corresponding to the k th user at m th subcarrier is

$$\mathbf{h}_k[m] = \gamma \underbrace{\left(\alpha_k^{m,1} \mathbf{a}(\theta_{k,m,1}) \right)}_{\text{LoS}} + \underbrace{\sum_{l=2}^L \alpha_k^{m,l} \mathbf{a}(\theta_{k,m,l})}_{\text{NLoS}} e^{-j2\pi\tau_{k,l}f_m}, \quad (3)$$

where $\gamma = \sqrt{\frac{N_{\text{T}}}{L}}$, $\alpha_k^{m,l} \in \mathbb{C}$ is the complex path gain, L is the total number of paths, and $\tau_{k,l}$ is the time delay of the l th path. $f_m = f_c + \frac{B}{M}(m - 1 - \frac{M-1}{2})$ is the m th subcarrier frequency with f_c and B being the carrier frequency and the bandwidth, respectively. The steering vector corresponding to the spatial channel direction $\theta_{k,m,l}$ defined for a uniform linear array is $N_{\text{T}} \times 1$ vector

$$\mathbf{a}(\theta_{k,m,l}) = \frac{1}{\sqrt{N_{\text{T}}}} [1, e^{-j\pi\theta_{k,m,l}}, \dots, e^{-j\pi(N_{\text{T}}-1)\theta_{k,m,l}}]^{\text{T}}, \quad (4)$$

where the spatial direction

$$\theta_{k,m,l} = \frac{2f_m}{c_0} d \vartheta_{k,l} = \frac{f_m}{f_c} \vartheta_{k,l}, \quad (5)$$

with $\vartheta = \sin \tilde{\vartheta}_{k,l}$ being the physical direction for the l -th path with $\tilde{\vartheta}_{k,l} \in [-\frac{\pi}{2}, \frac{\pi}{2}]$, c_0 is the speed of light, and $d = \frac{c_0}{2f_c}$ is the half-wavelength antenna spacing.

Note that $\theta_{k,m,l} \approx \vartheta_{k,l}$ when $f_m \approx f_c$ (see, e.g., Fig. 1). This observation allows us to employ frequency-independent analog beamformers (i.e., \mathbf{F}_{RF}) for $m \in \mathcal{M}$ in conventional mm-Wave

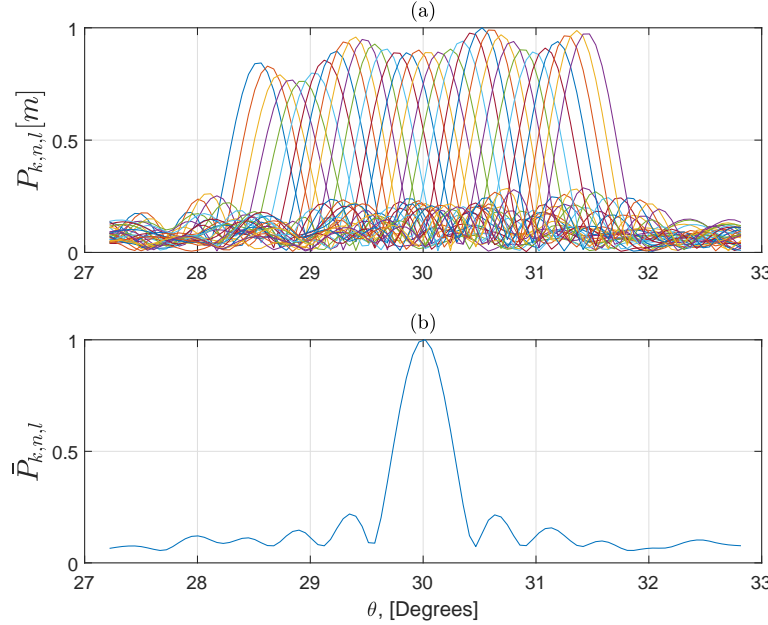


Fig. 1. Illustration of the beam-split effect in the beamspace for wideband THz scenario when $\vartheta = \frac{\pi}{6}$, $f_c = 300$ GHz, $B = 15$ GHz and $M = 32$. (a) deviated spectrum $P_{k,n,l}[m]$ for $m \in \mathcal{M}$ because of beam-split; (b) The aligned spectrum $\bar{P}_{k,n,l}$ after BSA.

systems. However, beam-split implies that with wider system bandwidth $|f_m - f_c|$, physical directions $\vartheta_{k,l}$ deviate from the spatial directions $\theta_{k,m,l}$.

Our goal is to estimate the THz channel $\mathbf{h}_k[m]$ for $m \in \mathcal{M}$ given the received pilot signals $y_k[m]$ in the presence of beam-split.

III. THZ CHANNEL ESTIMATION

Consider the downlink received signal model in (2). We assume a block-fading channel, wherein the coherence time is longer than the training time. Let $\tilde{\mathbf{f}}_j[m] \in \mathbb{C}^{N_T}$ be the beamformer vector, and the known pilot signals are $\tilde{\mathbf{S}}[m] = \text{diag}\{\tilde{s}_1[m], \dots, \tilde{s}_J[m]\} \in \mathbb{C}^{J \times J}$, where J is the number of pilot signals. Then, at the receiver side, each user collects the $J \times 1$ received signals as

$$\bar{\mathbf{y}}_k[m] = \tilde{\mathbf{S}}[m] \bar{\mathbf{F}}[m] \mathbf{h}_k[m] + \mathbf{n}_k[m], \quad (6)$$

where $\bar{\mathbf{F}} = \tilde{\mathbf{F}}^\top$, $\tilde{\mathbf{F}} = [\tilde{\mathbf{f}}_1[m], \dots, \tilde{\mathbf{f}}_J[m]]^\top \in \mathbb{C}^{J \times N_T}$ is beamformer matrix, $\bar{\mathbf{y}}_k = [y_k[1], \dots, y_k[M]]^\top$ and $\mathbf{n}_k = [n_k[1], \dots, n_k[M]]^\top$. Without loss of generality, by assuming $\bar{\mathbf{F}}[m] = \bar{\mathbf{F}}$ and $\tilde{\mathbf{S}}[m] = \mathbf{I}_J$,

(6) becomes

$$\bar{\mathbf{y}}_k[m] = \bar{\mathbf{F}}\mathbf{h}_k[m] + \mathbf{n}_k[m], \quad (7)$$

for which the least squares (LS) and MMSE solutions are readily

$$\begin{aligned} \mathbf{h}_k^{\text{LS}}[m] &= (\bar{\mathbf{F}}^H \bar{\mathbf{F}})^{-1} \bar{\mathbf{F}}^H \bar{\mathbf{y}}_k[m], \\ \mathbf{h}_k^{\text{MMSE}}[m] &= (\mathbf{R}_k^{-1}[m] + \bar{\mathbf{F}}^H \mathbf{R}_k^{-1}[m] \bar{\mathbf{F}})^{-1} \bar{\mathbf{F}}^H \bar{\mathbf{y}}_k[m], \end{aligned} \quad (8)$$

respectively, where $\mathbf{R}_k[m] = \mathbb{E}\{\mathbf{h}_k[m]\mathbf{h}_k^H[m]\}$ is the channel covariance matrix.

A. Sparse THz Channel Model

The main drawback of the conventional techniques in (8) is the requirement of overdetermined system, i.e., $J \geq N_T$, which results high channel training overheads due to the UM number of antennas. However, the THz channel is extremely sparse in the angular domain (i.e., $L \ll N_T$) due to high path loss as well as refraction and molecular absorption losses [4]. The angle domain representation of the channel, i.e., $\mathbf{x}_k[m] \in \mathbb{C}^N$ is

$$\mathbf{x}_k[m] = \mathbf{F}^H \mathbf{h}_k[m] = \gamma \sum_{l=1}^L \alpha_k^{m,l} \mathbf{u}_{k,m,l} e^{-j2\pi\tau_{k,l} f_m}, \quad (9)$$

where $\mathbf{F} \in \mathbb{C}^{N_T \times N}$ is an overcomplete discrete Fourier transform (DFT) matrix covering the whole angular domain with the resolution of $\rho = \frac{1}{2N}$. The n -th column of \mathbf{F} is the steering vector $\mathbf{a}(\phi_n) \in \mathbb{C}^{N_T}$ with $\phi_n = \frac{2n-N-1}{N}$ for $n = 1, \dots, N$. $\mathbf{u}_{k,m,l} \in \mathbb{C}^N$ denotes the channel support vector corresponding to the angle domain representation with

$$\mathbf{u}_{k,m,l} = \mathbf{F}^H \mathbf{a}(\theta_{k,m,l}) = [\Sigma(\theta_{k,m,l} - \phi_1), \dots, \Sigma(\theta_{k,m,l} - \phi_N)]^T, \quad (10)$$

where $\Sigma(a) = \frac{\sin N\pi a/2}{\sin \pi a/2}$ is the Dirichlet sinc function. Due to the power-focusing capability of $\Sigma(a)$, most of the power is focused on only small number of elements in the beamspace corresponding to the channel support [4, 6]. Therefore, $\mathbf{x}_k[m]$ is a sparse vector with sparsity level L , i.e., $\|\mathbf{x}_k[m]\|_0 = L$, and the channel vector $\mathbf{h}_k[m]$ is approximated as $\hat{\mathbf{h}}_k[m] \approx \mathbf{F}\mathbf{x}_k[m]$.

Now, consider the following underdetermined system, i.e.,

$$\mathbf{y}_k[m] = \mathbf{B}\mathbf{F}\mathbf{x}_k[m] + \mathbf{n}_k[m], \quad (11)$$

where $\mathbf{B} \in \mathbb{C}^{N_{\text{RF}} \times N_{\text{T}}}$ is a frequency-independent matrix representing the precoder at the BS, hence we have $|[\mathbf{B}]_{i,j}| = \frac{1}{\sqrt{N_{\text{T}}}}$. Exploiting the sparsity of $\mathbf{x}_k[m]$ in (11), we formulate the following sparse recovery (SR) problem

$$\begin{aligned} \hat{\mathbf{x}}_k[m] &= \arg \min_{\mathbf{x}_k[m]} \|\mathbf{x}_k[m]\|_1 \\ \text{subject to: } &\|\mathbf{y}_k[m] - \mathbf{A}\mathbf{x}_k[m]\|_2^2 \leq \epsilon, \end{aligned} \quad (12)$$

where $\mathbf{A} = \mathbf{B}\mathbf{F} \in \mathbb{C}^{N_{\text{RF}} \times N}$ and the residual ϵ is bounded with $\epsilon \leq \sigma_n \sqrt{N_{\text{RF}} + \zeta \sqrt{2N_{\text{RF}}}}$, where ζ is an adjustable parameter controlling the noise power $\mathbb{E}\{\|\mathbf{n}_k[m]\|_2^2\}$ [6, 13]. The sparsity of $\mathbf{x}_k[m]$ allows us to estimate $\mathbf{h}_k[m]$ with much less observations and pilot signals, i.e., $J = N_{\text{RF}} \ll N_{\text{T}}$. Using $\hat{\mathbf{x}}_k[m]$, the channel is estimated as $\hat{\mathbf{h}}_k^{\text{SR}}[m] = \mathbf{F}\hat{\mathbf{x}}_k[m]$.

B. Beamspace Support Alignment

Due to the frequency-independent structure of \mathbf{A} , the spatial directions $\theta_{k,m,l}$ corresponding to the support of $\mathbf{x}_k[m]$ are deviated from the physical direction $\vartheta_{k,l}$ due to beam-split (see Fig. 1(a)). Hence, the above sparse recovery techniques will not yield accurate results. In the proposed method, we align the deviated support of $\mathbf{x}_k[m]$ with respect to m and generate a single beamspace spectrum for accurate channel and direction estimation.

We start by determining the amount of index mismatch in the beamspace between the spatial and physical directions. Hence, we first compute the index $n_{k,m,l}^*$ corresponding to the l th spatial channel direction corresponding to the k th user and the m th subcarrier as

$$n_{k,m,l}^* = \arg \max_n P_{k,n,l}[m], \quad (13)$$

where $P_{k,n,l}[m] = |\mathbf{A}_n^H \mathbf{r}_{l,k}[m]|$ corresponds to the beamspace spectrum for the m th subcarrier. $\mathbf{r}_{l,k}[m]$ is the residual observation vector and equals to $\mathbf{y}_k[m]$ for $l = 1$, and $\mathbf{A}_n \in \mathbb{C}^{N_{\text{RF}}}$ denotes the n th column of \mathbf{A} . Then, the l th spatial direction $\theta_{k,m,l}$ is $\theta_{k,m,l} = \phi_{n_{k,m,l}^*}$. In order to find the physical direction, we first compute the index mismatch due to beam-split as

$$\Delta_{k,m,l} = \lceil (1 - \frac{f_m}{f_c}) \frac{\phi_{n_{k,m,l}^*}}{\rho} \rceil, \quad (14)$$

which measures the number of indices between the physical and spatial directions defined in (5). By shifting $P_{k,n,l}[m]$ by $\Delta_{k,m,l}$, we obtain the beam-split corrected spectrum as $\tilde{P}_{k,n,l}[m] = P_{k,n-\Delta_{k,m,l},l}[m]$ which is the circularly shifted version of $P_{k,n,l}[m]$. In order to capture most of

Algorithm 1 Beamspace Support Alignment

Input: \mathbf{A} , ρ , $\mathbf{y}_k[m]$, f_m for $m \in \mathcal{M}$.

Output: $\hat{\mathbf{h}}_k[m]$.

1: **for** $k \in \{1, \dots, K\}$

2: Initialize: $l = 1, \mathcal{I}_{l-1,k}[m] = \emptyset, \mathbf{r}_{l,k}[m] = \mathbf{y}_k[m]$ for $m \in \mathcal{M}$.

3: **while** $l \leq L$

4: **for** $m \in \mathcal{M}$

5: $P_{k,n,l}[m] = |\mathbf{A}_n^H \mathbf{r}_{l,k}[m]|$ for $n = 1, \dots, N$.

6: $n_{k,m,l}^* = \arg \max_n P_{k,n,l}[m]$.

7: $\Delta_{k,m,l} = \lceil (1 - \frac{f_m}{f_c}) \frac{\phi_{n_{k,m,l}^*}}{\rho} \rceil$.

8: $\tilde{P}_{k,n,l}[m] = P_{k,n-\Delta_{k,m,l}}[m]$.

9: $\theta_{k,m,l} = \phi_{n_{k,m,l}^*}$.

10: **end for**

11: $\bar{P}_{k,n,l} = \sum_{m=1}^M \tilde{P}_{k,n,l}[m]$ for $n = 1, \dots, N$.

12: $\bar{n}_{k,l}^* = \arg \max_n \bar{P}_{k,n,l}$. $\vartheta_{k,l} = \phi_{\bar{n}_{k,l}^*}$.

13: **for** $m \in \mathcal{M}$

14: $\mathcal{I}_{l,k}[m] = \mathcal{I}_{l-1,k}[m] \cup \{\bar{n}_{k,l}^* - \Delta_{k,m,l}\}$.

15: $\mathbf{r}_{l+1,k}[m] = \mathbf{r}_{l,k}[m] - \mathbf{A}_{\mathcal{I}_{l+1,k}[m]} \mathbf{A}_{\mathcal{I}_{l+1,k}[m]}^H \mathbf{y}_k[m]$.

16: **end for**

17: $l \leftarrow l + 1$.

18: **end while**

19: $\Xi_k[m] = \mathcal{I}_{1,k}[m] \cup \mathcal{I}_{2,k}[m], \dots, \cup \mathcal{I}_{L,k}[m]$.

20: $\hat{\mathbf{x}}_k[m] = \mathbf{A}_{\Xi_k[m]}^H \mathbf{y}_k[m]$.

21: $\hat{\mathbf{h}}_k[m] = \mathbf{F} \hat{\mathbf{x}}_k[m]$.

22: **end for**

the power distributed across all subcarriers due to beam-split and exploit multi-carrier channels, we incorporate the shifted beamspace spectrum for $m \in \mathcal{M}$ as

$$\bar{P}_{k,n,l} = \sum_{m=1}^M \tilde{P}_{k,n,l}[m], \quad (15)$$

which generates a single spectrum as illustrated in Fig. 1(b).

Next, we obtain the l th physical channel direction $\vartheta_{k,l}$ as $\vartheta_{k,l} = \phi_{\bar{n}_{k,m}^*}$, where $\bar{n}_{k,l}^* = \arg \max_n \bar{P}_{k,n}$. Combining the indices of directions in the set $\Xi_k[m]$ as $\Xi_k[m] = \bigcup_{l=1}^L \bar{n}_{k,l}^* - \Delta_{k,m,l}$, the support vector is

$$\hat{\mathbf{x}}_k[m] = \mathbf{A}_{\Xi_k[m]}^\dagger \mathbf{y}_k[m], \quad (16)$$

for which, we obtain the channel estimate as $\hat{\mathbf{h}}_k[m] = \mathbf{F} \hat{\mathbf{x}}_k[m]$. The algorithmic steps of our proposed BSA approach are summarized in Algorithm 1. Using the channel estimate via BSA, we develop an FL scheme for THz channel estimation in the following.

IV. FL-BASED THZ CHANNEL ESTIMATION

In FL, the users collaborate on training a learning model by computing the model parameters based on their local datasets [18, 19]. Let $\boldsymbol{\theta} \in \mathbb{R}^Q$ and \mathcal{D}_k be the set of model parameters and the local dataset of the k th user, respectively. Then, the trained model provides a nonlinear relationship, $f(\boldsymbol{\theta})$ between the input and output as $\mathcal{Y}_k^{(i)} = f(\boldsymbol{\theta}) \mathcal{X}_k^{(i)}$ for $i = 1, \dots, \mathsf{D}_k$, where $\mathsf{D}_k = |\mathcal{D}_k|$ is the number of samples in the k th local dataset. Here, $\mathcal{X}_k^{(i)}$ and $\mathcal{Y}_k^{(i)}$ are the input and output data for the i th sample of the k th dataset with $\mathcal{D}_k^{(i)} = (\mathcal{X}_k^{(i)}, \mathcal{Y}_k^{(i)})$.

A. Data Collection and Training

During dataset collection, each user collects its own training dataset from the received pilots. For labeling, we consider two different cases, i.e., channel estimates via MMSE and BSA (see Sec. V). Given the channel estimate $\hat{\mathbf{h}}_k[m]$, the output data is given by

$$\mathcal{Y}_k = \left[\text{Re}\{\hat{\mathbf{h}}_k[m]\}^\top, \text{Im}\{\hat{\mathbf{h}}_k[m]\}^\top \right]^\top \in \mathbb{R}^{2N_T}. \quad (17)$$

The input data $\mathcal{X}_k \in \mathbb{R}^{N_{RF} \times 3}$ includes the real, imaginary and angle information of $\mathbf{y}_k[m]$ to yield improved feature representation [18]. Thus, we have $[\mathcal{X}_k]_1 = \text{Re}\{\mathbf{y}_k[m]\}$, $[\mathcal{X}_k]_2 = \text{Im}\{\mathbf{y}_k[m]\}$ and $[\mathcal{X}_k]_3 = \angle\{\mathbf{y}_k[m]\}$.

Then, the FL problem becomes

$$\begin{aligned} \min_{\boldsymbol{\theta}} \quad & \frac{1}{K} \sum_{k=1}^K \mathcal{L}_k(\boldsymbol{\theta}) \\ \text{subject to: } \quad & f(\mathcal{X}_k^{(i)} | \boldsymbol{\theta}) = \mathcal{Y}_k^{(i)}, \end{aligned} \quad (18)$$

for $i = 1, \dots, \mathsf{D}_k$ and $k = 1, \dots, K$. In (18),

$$\mathcal{L}_k(\boldsymbol{\theta}) = \frac{1}{\mathsf{D}_k} \sum_{i=1}^{\mathsf{D}_k} \|f(\mathcal{X}_k^{(i)} | \boldsymbol{\theta}) - \mathcal{Y}_k^{(i)}\|_{\mathcal{F}}^2, \quad (19)$$

corresponds to the loss function at the k th user and $f(\mathcal{X}_k^{(i)} | \boldsymbol{\theta})$ denotes model prediction given the input $\mathcal{X}_k^{(i)}$. To efficiently solve (18), gradient descent is employed and the problem is solved iteratively, wherein model parameter update is performed at the t th iteration as

$$\boldsymbol{\theta}_{t+1} = \boldsymbol{\theta}_t - \eta \frac{1}{K} \sum_{k=1}^K \boldsymbol{\beta}_k(\boldsymbol{\theta}_t), \quad (20)$$

for $t = 1, \dots, T$. Here, $\boldsymbol{\beta}_k(\boldsymbol{\theta}_t) = \nabla \mathcal{L}_k(\boldsymbol{\theta}_t) \in \mathbb{R}^Q$ is the gradient vector and η is the learning rate.

During model training, each user transmits the model update vector $\boldsymbol{\beta}_k(\boldsymbol{\theta}_t)$ to the BS. Assume that the model $\boldsymbol{\beta}_k(\boldsymbol{\theta}_t)$ is divided into $V = \frac{Q}{M}$ equal-length blocks for each subcarrier as

$$\boldsymbol{\beta}_k(\boldsymbol{\theta}_t) = [\mathbf{x}_K^{(t)\top}[1], \dots, \mathbf{x}_K^{(t)\top}[M]]^\top, \quad (21)$$

where $\mathbf{x}_k^{(t)}[m] \in \mathbb{C}^V$ corresponds to the transmitted symbols of the k th user. Then, the received signal for the t th iteration at the BS in the uplink, i.e., $\mathbf{Y}^{(t)}[m] \in \mathbb{C}^{N_{\text{T}} \times V}$ becomes

$$\mathbf{Y}^{(t)}[m] = \sum_{k=1}^K \mathbf{h}_k^{(t)}[m] \mathbf{x}_k^{(t)\top}[m] + \mathbf{N}[m], \quad (22)$$

where $\mathbf{h}_k^{(t)}[m] \in \mathbb{C}^{N_{\text{T}}}$ and $\mathbf{N}[m] \in \mathbb{C}^{K \times V}$ denote the uplink channel vector and noise matrix, respectively.

B. Communications Overhead and Complexity

The communications overhead of both FL and CL can be given as the amount of data transmitted during training [17, 19], i.e., $\mathcal{T}_{\text{FL}} = 2QTK$ and $\mathcal{T}_{\text{CL}} = \sum_{k=1}^K \mathsf{D}_k(3N_{\text{RF}} + 2N_{\text{T}})$, respectively. Here, \mathcal{T}_{FL} involves transmission of model parameters of K users for T iteration, while \mathcal{T}_{CL} is computed as the size of dataset of K users.

We also discuss the computational complexity of the proposed BSA approach, which is mainly due to matrix multiplications in the steps 5 ($O(MN^2)$), 15 ($O(MN_{\text{RF}}^2 N^3)$), 20 ($O(MN_{\text{RF}} N)$) and 21 ($O(MN_{\text{T}} N)$) of Algorithm 1, respectively. Hence, the combined time complexity of the BSA approach is $O(MN(N(1 + N_{\text{RF}}^2 N) + N_{\text{RF}} + N_{\text{T}}))$.

V. NUMERICAL EXPERIMENTS

In the simulations, the THz channel scenario is realized based on the channel model in (3) with $f_c = 300$ GHz, $B = 15$ GHz, $M = 128$, $N_T = 1024$, $N_{RF} = 32$, $L = 5$, $K = 8$ and $\vartheta_{k,l} \in [-\frac{\pi}{2}, \frac{\pi}{2}]$ [2–5, 12]. The overcomplete dictionary matrix \mathbf{F} is constructed for $N = 3N_T$, and $[\mathbf{B}]_{i,j} = \frac{1}{\sqrt{N_T}}e^{j\varphi}$, where $\varphi \sim \text{uniform}(-\frac{\pi}{2}, \frac{\pi}{2})$.

Data generation and training are handled over an hyperparameter optimization of the learning model in the FL toolbox in MATLAB on a PC with a 2304-core GPU. We design a CNN with 12 layers and $Q = 603,648$ parameters [17]. The first layer accepts the input of size $N_{RF} \times 3$. The $\{2, 4, 6, 8\}$ th layers are convolutional layers with 128 filters of size 3×3 . The $\{3, 5, 7, 9\}$ th layers are normalization layers. The 10th layer is a fully connected layer with 1024 units, following with a dropout layer with 50% probability. Finally, the 12th layer is the output layer of size $2N_T \times 1$. The CNN model is trained for $T = 100$ iterations with the learning rate $\eta = 0.001$. During data generation, we generated $V = 100$ channel realizations, and we added AWGN on the input data for three signal-to-noise ratio (SNR) levels, i.e., $\text{SNR} = \{15, 20, 25\}$ dB for $G = 50$ realizations to provide robust performance [17].

Fig. 2 shows the channel estimation performance of our proposed approach in comparison with the state-of-the-art techniques, e.g., MMSE in (8), generalized simultaneous orthogonal matching pursuit (GSOMP) [13], SR in (12), BSPD [12], DCCN [15] and generative adversarial network (GAN) [11], in terms of normalized MSE (NMSE), calculated as $\text{NMSE} = \frac{1}{J_T K M} \sum_{i=1, k=1, m=1}^{J_T, K, M} \frac{\|\mathbf{h}_k[m] - \hat{\mathbf{h}}_k^{(i)}[m]\|_2^2}{\|\mathbf{h}_k[m]\|_2^2}$, where $J_T = 500$ is the number of Monte Carlo trials. We implemented the proposed FL scheme with two different labeling methods, i.e., MMSE and BSA. We observe that the proposed FL-BSA approach achieves better NMSE as compared to the existing model-based (BSPD and SR) and model-free (GAN and DCCN) techniques, and closely follows GSOMP. Note that the GSOMP method needs an additional hardware to generate virtual array response for $f_m \neq f_c$ for $m \in \mathcal{M}$, while the proposed approach does not involve such hardware requirement. The effectiveness of the proposed method is attributed to the mitigation of beam-split via support alignment with high resolution channel direction estimates. The remaining methods, i.e. SR, GAN and DCCN, do not take into account the effect of beam-split for THz channel estimation. While the BSPD approach is designed to mitigate the beam-split, it fails to collect the accurate supports related to the aligned beampulse spectrum and suffers from poor physical direction estimates due to the use of low resolution dictionary.

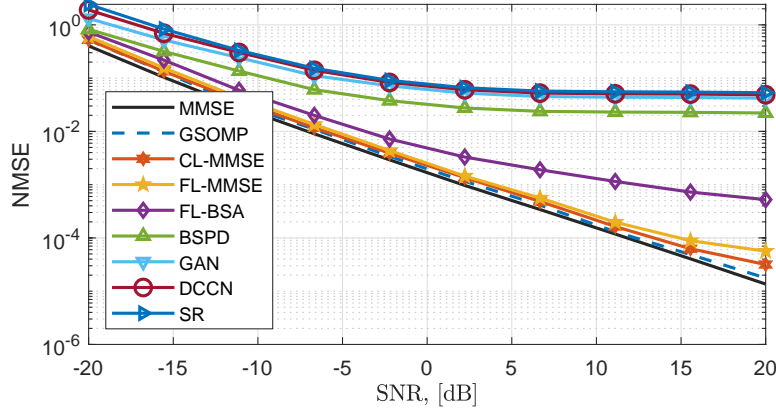


Fig. 2. Channel estimation performance versus SNR.

In Fig. 3, we present the NMSE performance with respect to number of pilots J . We note that the the proposed approach achieves much lower channel estimation levels as compared to BSPD and SR.

Next, we analyze the communications overhead for the proposed approach in terms of number of transmitted data symbols. According to the analysis in Sec. IV-B, the communications overhead of CL is computed as $\mathcal{T}_{\text{CL}} = 8 \cdot D_k \cdot (3 \cdot 32 + 2 \cdot 1024) = 65.8 \times 10^9$, where the number of input-output tuples in the dataset is $D_k = 3MVG = 3 \cdot 128 \cdot 100 \cdot 50 = 3.8 \times 10^6$. On the other hand, the communications overhead of FL is $\mathcal{T}_{\text{FL}} = 2 \cdot 603,648 \cdot 100 \cdot 8 = 0.96 \times 10^9$, which exhibits approximately 68 times lower than that of CL. Thus, the proposed FL approach is an efficient tool especially for THz-related datasets, which usually involve large number of antennas.

VI. CONCLUSIONS

In this paper, we introduced an FL approach for THz channel estimation. The proposed approach is advantageous in terms of communications overhead and enjoys approximately 68 times lower overhead than that of centralized schemes. Furthermore, we proposed BSA technique to align the deviated beamspace spectrum of multiple subcarriers and mitigate the effect of beam-split without requiring additional hardware components.

REFERENCES

- [1] K. B. Letaief, Y. Shi, J. Lu, and J. Lu, “Edge artificial intelligence for 6G: Vision, enabling technologies, and applications,” *IEEE J. Sel. Areas Commun.*, vol. 40, no. 1, pp. 5–36, 2021.

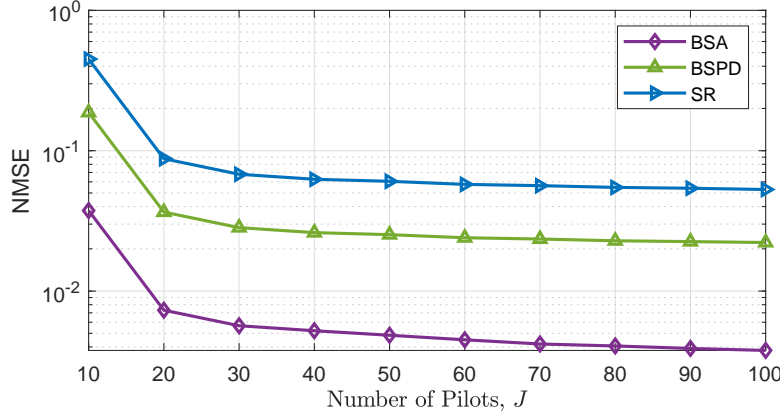


Fig. 3. Channel estimation performance versus number of pilots.

- [2] A. M. Elbir, K. V. Mishra, and S. Chatzinotas, “Terahertz-Band Joint Ultra-Massive MIMO Radar-Communications: Model-Based and Model-Free Hybrid Beamforming,” *IEEE J. Sel. Top. Signal Process.*, vol. 15, no. 6, pp. 1468–1483, Oct. 2021.
- [3] H. Sarieddeen, M.-S. Alouini, and T. Y. Al-Naffouri, “An overview of signal processing techniques for Terahertz communications,” *Proceedings of the IEEE*, vol. 109, no. 10, pp. 1628–1665, 2021.
- [4] H. Yuan, N. Yang, K. Yang, C. Han, and J. An, “Hybrid Beamforming for Terahertz Multi-Carrier Systems Over Frequency Selective Fading,” *IEEE Trans. Commun.*, vol. 68, no. 10, pp. 6186–6199, Jul 2020.
- [5] J. Tan and L. Dai, “Wideband Beam Tracking in THz Massive MIMO Systems,” *IEEE J. Sel. Areas Commun.*, vol. 39, no. 6, pp. 1693–1710, Apr 2021.
- [6] B. Wang, M. Jian, F. Gao, G. Y. Li, and H. Lin, “Beam Squint and Channel Estimation for Wideband mmWave Massive MIMO-OFDM Systems,” *IEEE Trans. Signal Process.*, vol. 67, no. 23, pp. 5893–5908, Oct. 2019.
- [7] L. Dai, J. Tan, Z. Chen, and H. V. Poor, “Delay-Phase Precoding for Wideband THz Massive MIMO,” *IEEE Trans. Wireless Commun.*, p. 1, Mar. 2022.
- [8] A. Brighente, M. Cerutti, M. Nicoli, S. Tomasin, and U. Spagnolini, “Estimation of Wideband Dynamic mmWave and THz Channels for 5G Systems and Beyond,” *IEEE J. Sel. Areas Commun.*, vol. 38, no. 9, pp. 2026–2040, Jun 2020.
- [9] S. Srivastava, A. Tripathi, N. Varshney, A. K. Jagannatham, and L. Hanzo, “Hybrid Transceiver Design for Tera-Hertz MIMO Systems Relying on Bayesian Learning Aided Sparse Channel Estimation,” *arXiv*, Sep. 2021.
- [10] W. Yu, Y. Shen, H. He, X. Yu, J. Zhang, and K. B. Letaief, “Hybrid Far- and Near-Field Channel Estimation for THz Ultra-Massive MIMO via Fixed Point Networks,” *arXiv*, May 2022.
- [11] E. Balevi and J. G. Andrews, “Wideband Channel Estimation With a Generative Adversarial Network,” *IEEE Trans. Wireless Commun.*, vol. 20, no. 5, pp. 3049–3060, Jan. 2021.
- [12] J. Tan and L. Dai, “Wideband channel estimation for THz massive MIMO,” *China Commun.*, vol. 18, no. 5, pp. 66–80, May 2021.
- [13] K. Dovelos, M. Matthaiou, H. Q. Ngo, and B. Bellalta, “Channel Estimation and Hybrid Combining for Wideband Terahertz Massive MIMO Systems,” *IEEE J. Sel. Areas Commun.*, vol. 39, no. 6, pp. 1604–1620, Apr. 2021.
- [14] S. Nie and I. F. Akyildiz, “Deep Kernel Learning-Based Channel Estimation in Ultra-Massive MIMO Communications at 0.06-10 THz,” in *2019 IEEE Globecom Workshops (GC Wkshps)*. IEEE, Dec. 2019, pp. 1–6.

- [15] Y. Chen and C. Han, "Deep CNN-Based Spherical-Wave Channel Estimation for Terahertz Ultra-Massive MIMO Systems," in *GLOBECOM 2020 - 2020 IEEE Global Communications Conference*. IEEE, Dec. 2020, pp. 1–6.
- [16] Z. Li, Z. Chen, X. Ma, and W. Chen, "Channel Estimation for Intelligent Reflecting Surface Enabled Terahertz MIMO Systems: A Deep Learning Perspective," in *2020 IEEE/CIC International Conference on Communications in China (ICCC Workshops)*. IEEE, Aug. 2020, pp. 75–79.
- [17] A. M. Elbir and S. Coleri, "Federated Learning for Channel Estimation in Conventional and RIS-Assisted Massive MIMO," *IEEE Trans. Wireless Commun.*, vol. 21, no. 6, pp. 4255–4268, Nov. 2021.
- [18] A. M. Elbir, A. K. Papazafeiropoulos, and S. Chatzinotas, "Federated Learning for Physical Layer Design," *IEEE Commun. Mag.*, vol. 59, no. 11, pp. 81–87, Nov. 2021.
- [19] H. B. McMahan, E. Moore, D. Ramage, S. Hampson, and B. A. y. Arcas, "Communication-Efficient Learning of Deep Networks from Decentralized Data," *arXiv*, Feb 2016.